Nuclear Instruments and Methods in Physics Research A 849 (2017) 49–54

Contents lists available at ScienceDirect

Nuclear Instruments and Methods in Physics Research A

journal homepage: www.elsevier.com/locate/nima

Implementation of the n-body Monte-Carlo event generator into the Geant4 toolkit for photonuclear studies

Wen Luo[a,*], Hao-yang Lan[a], Yi Xu[b], Dimiter L. Balabanski[b]

[a] School of Nuclear Science and Technology, University of South China, Hengyang 421001, China
[b] Extreme Light Infrastructure-Nuclear Physics, "Horia Hulubei" National Institute for Physics and Nuclear Engineering (IFIN-HH), 30 Reactorului, 077125 Bucharest-Magurele, Romania

ARTICLE INFO

Keywords:
Photonuclear reactions
Particle sources and targets
Monte Carlo simulations
Medical radioisotopes

ABSTRACT

A data-based Monte Carlo simulation algorithm, Geant4-GENBOD, was developed by coupling the n-body Monte-Carlo event generator to the Geant4 toolkit, aiming at accurate simulations of specific photonuclear reactions for diverse photonuclear physics studies. Good comparisons of Geant4-GENBOD calculations with reported measurements of photo-neutron production cross-sections and yields, and with reported energy spectra of the ^{6}Li(n,α)*t* reaction were performed. Good agreements between the calculations and experimental data were found and the validation of the developed program was verified consequently. Furthermore, simulations for the ^{92}Mo(γ,p) reaction of astrophysics relevance and photo-neutron production of ^{99}Mo/^{99m}Tc and ^{225}Ra/^{225}Ac radioisotopes were investigated, which demonstrate the applicability of this program. We conclude that the Geant4-GENBOD is a reliable tool for study of the emerging experiment programs at high-intensity γ-beam laboratories, such as the Extreme Light Infrastructure – Nuclear Physics facility and the High Intensity Gamma-Ray Source at Duke University.

1. Introduction

Photonuclear reactions with emission of neutrons, protons and α-particles are of paramount importance in fundamental research and industrial applications, such as studies of astrophysical processes [1–3], transmutation of long-lived radionuclides [4–7], production of medical radioisotopes [8–11], boron neutron capture therapy [12,13], and radiography and radiotherapy [14–16]. For the production of medical radioisotopes by photonuclear reactions, it is crucial to estimate accurately the photonuclear yield and to obtain reliable estimates of the specific activity for the produced radioisotopes [17]. For the purposes of radiation protection, it is essential to evaluate the production of photo-neutrons precisely in medical diagnostics and therapy. These photo-neutrons usually arise from energetic γ-rays penetrating high-*Z* materials and may cause unintended radiation exposure of patients and staff.

Currently, Geant4 [18,19], FLUKA [20], and MCNP [21] are the most common Monte Carlo radiation transport codes, which are used for the photonuclear reaction studies. Geant4 allows microscopic Monte Carlo simulations of particles interacting with the materials and it has been widely used for predictions of the required yields, optimizations of the experimental setups, estimates of the secondary effects, calculations of radiation shielding, *etc.* However, the hadronic model in Geant4 fails to reproduce accurately some experimental photonuclear reaction cross-sections [22,23], which may largely restrict the Geant4-based simulations of photonuclear experiments. First of all, it is due to the lack of sufficient experimental data for large-scale benchmarking tests. In addition, the hadronic models implemented in Geant4 were developed for general use and none of them is specialized for specific reactions, *e.g.* the ^{9}Be(p,n)^{9}B reaction [24]. Similarly, other simulation toolkits such as FLUKA also confront such a dilemma, even if well-tested models are used, optimized in comparison with measurements. In short, the usage of these simulation toolkits for photonuclear studies suffers limitations.

Recently, a data-based photonuclear reaction model [23] and a new-charge exchange model [24] have been developed for accurate simulations of photo-neutron reactions and of the proton-induced reaction ^{9}Be(p,n)^{9}B, respectively, and were implemented in their local copies of the Geant4. The main contribution of this approach is the inclusion of photon- or proton-induced reactions by using the evaluated data, photonuclear data from ENDF/B-VII.1 [25] as the input. The next step along this line was the development of a data-based photonuclear reaction simulation algorithm [17], aiming to predict accurately photo-neutron or photo-proton production and estimate the

* Corresponding author.
E-mail address: wenluo-ok@163.com (W. Luo).

http://dx.doi.org/10.1016/j.nima.2017.01.010
Received 30 November 2016; Received in revised form 22 December 2016; Accepted 3 January 2017
Available online 04 January 2017

specific activity of isotopes produced in photonuclear reactions [10,11].

In this work, we report a data-based Monte Carlo approach for the studies of photonuclear reactions, which utilizes the n-body Monte-Carlo event generator and standard electromagnetic package within the Geant4 simulation toolkit. This approach uses as an input photonuclear cross-section data from evaluated or experimental databases and aims at accurate simulations of specific photonuclear reactions for diverse photonuclear physics studies. The validity of this approach is verified by accurate reproduction of experimental photo-neutron reaction cross-sections, yields and spectral distributions within a broad energy region covering the giant dipole resonance (GDR). The outline of the paper is as follows. In Section 2 the simulation tools are summarized. In Section 3 benchmark simulation results obtained with the developed routine are presented. Potential application of this approach for nuclear astrophysics studies and for medical radioisotope research, related to the emerging experimental program at the Extreme Light Infrastructure Nuclear Physics (ELI-NP) facility, is discussed in Section 4, and the summary is provided in Section 5.

2. Simulation tools

Geant4 is an open source platform for the simulation of nuclear and particle experiments, which includes comprehensive physics processes and databases of particle–matter interactions. It has been thoroughly tested and is being widely used in various scientific fields. These fields include high energy, nuclear and accelerator physics, as well as studies in medical and space science. More information, validations and detailed descriptions of the software toolkit can be found at the Geant4 website [26].

2.1. Photonuclear model in Geant4 (v4.9.6)

For the simulations of photonuclear interactions, two alternatives are provided in Geant4 (v4.9.6). One uses the G4PhotoNuclearProcess class [27] and the other is based on the G4GammaNuclearReaction model [28]. Note that the G4GammaNuclearReaction is dropped from Geant4 in release 10.0 and later. The G4PhotoNuclearProcess handles inelastic photon scattering from nuclei. They include the G4PhotoNuclearCrossSection class [29], providing estimates of the total inelastic cross-sections for photonuclear interactions with nuclei and the G4CascadeInterface class [30], which simulates final states for photonuclear reactions. The G4GammaNuclearReaction also invokes the G4PhotoNuclearCrossSection class, but uses the Chiral Invariant Phase Space Model (CHIPS) model [31] to generate the final states for gamma-nuclear inelastic scattering. Although these processes (models) should be valid for photons within the energy range of $0 \le E_\gamma < 3.5$ GeV, they have been tested only in the higher energy range 60 MeV–3 GeV [30].

2.2. Geant4-GENBOD

The implementation in Geant4 a physical process includes two modules: the first generates the final state particles and their kinematic distributions, and the second calculates the reaction cross-section and the mean free path in various materials. According to the modular structure, Geant4-GENBOD was developed in our study.

GENBOD, W515 from CERNLIB [32], is an n-body Monte-Carlo event generator. It uses the method of Raubold and Lynch [33] and can generate a multi-particle weighted event within a Lorentz-invariant Fermi phase space. The total center-of-mass (CM) energy as well as the number and the masses of the outgoing particles are specified by the user, but may be changed from event to event. Using the definitions of GENBOD, the TGenPhaseSpace class [34] has been specified and successfully implemented in ROOT [35], which is a modular scientific software framework and provides all the functionalities for addressing big-data processing, statistical analysis, visualization and data storage.

The TGenPhaseSpace class was invoked to facilitate the aforementioned first module. For specific photonuclear reaction, the n-body events were generated in the CM frame. The number and the masses of the decay products were specified and their CM energies and momentum vectors were calculated. Since the quantities of the decay products were determined in the parent particle CM frame, we boosted to the frame where the parent is moving, by using the velocity β of the parent particle. The final state particles and their kinematic distributions were obtained accordingly and these particles were regarded as dynamic particles in Geant4.

The second module included the input of the required photonuclear data. The data can be taken directly from EXFOR database [38], whenever experimental data are available. Photonuclear response can also be calculated with EMPIRE [36] or TALYS [37]. Comparisons between them are further needed, which enables to select reliable photonuclear data. Then the cross-section data was written into an external file or as a hard-coded one for further uses. Note that a linear interpolation method was employed to calculate reaction cross-section for arbitrary incoming photon. Afterwards, the free mean paths for photonuclear processes were calculated.

The Geant4-GENBOD approach was used for modeling of photonuclear reactions. Results from simulations were crosschecked and compared with the EXFOR database and with simulations within the Geant4 toolkit, using different approaches described earlier. The results obtained from the Geant4-GENBOD program are hereafter simply referred to as G4-GENBOD. The EXFOR data used for benchmarking tests are referred to as EXFOR. Simulations within the Geant4, which use the G4PhotoNuclearProcess class and the G4GammaNuclearReaction class, are referred to as G4PNP and G4GNR, respectively.

3. Results and discussions

3.1. Cross-sections of photonuclear reactions

Simulations of photo-neutron production were performed for ^{9}Be, ^{100}Mo and ^{197}Au. ^{9}Be is a light nucleus, for which the photo-neutron reaction occurs at low energies due to the low neutron separation energy of 1.66 MeV. Experimentally, low-energy bremsstrahlung radiation and quasi-monochromatic γ-ray beams produced in the inverse Compton scattering of laser photons have been used for such studies [39,40]. ^{100}Mo has been chosen from the intermediate-mass region due to the considerably large (γ,n) reaction cross-section, and ^{197}Au was chosen from the heavy-mass region due to the large (γ,n) reaction cross-section. For the computation of photonuclear reaction cross-sections, a cylindrical 1.0-mm thick target with a radius of 4.5 cm radius was considered, thus achieving approximately a semi-infinite geometry.

The results for ^{9}Be(γ,n) and ^{9}Be(γ,2 n) reaction cross-sections are shown in Fig. 1. Good agreement was found between the G4-GENBOD results and EXFOR data for the photo-neutron reaction cross-sections in the GDR region, which corresponds to the incident photon energies of $E_\gamma \le 35$ MeV. However, large discrepancies can be observed between the G4PNP simulations and EXFOR data for both of the (γ,n) and (γ,2n) reaction cross-sections in the GDR region. For ^{9}Be(γ,n) reaction, the G4PNP results fail to reproduce the low-energy peak of the cross-section and underestimate it by up to three orders of magnitude in the region of incident photon energies $E_\gamma \le 15$ MeV. Such discrepancy is due to an underestimation of photo-neutron production for the ^{9}Be(γ,n) reaction, as discussed later. For the ^{9}Be(γ,2 n) reaction, the G4PNP calculations underestimate the experimental values in the cross-section region by a factor of ten. The available data for the cross-sections of

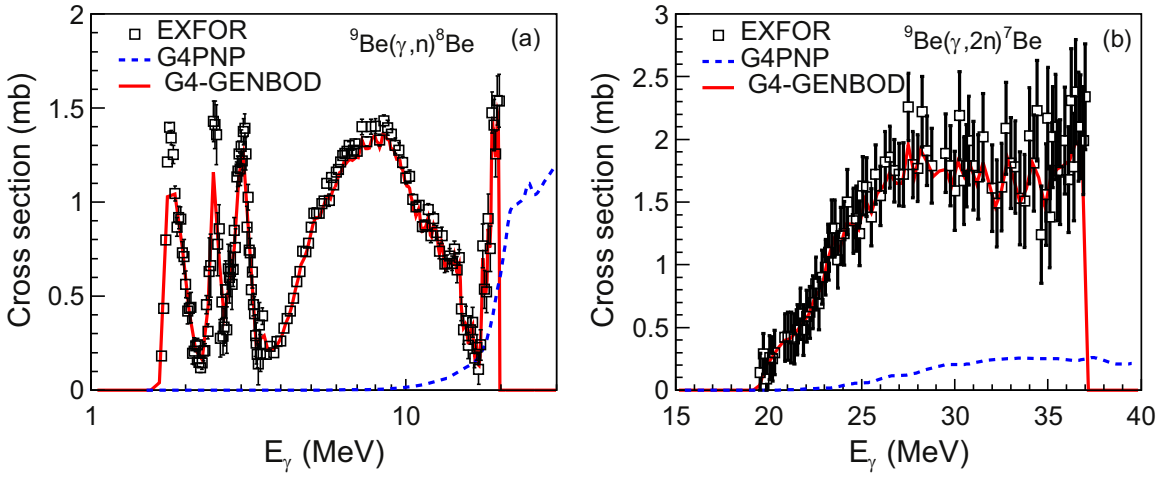

Fig. 1. Reaction cross-section for (a) the (γ, n) reaction and for (b) the (γ,2n) reactions on the ^{9}Be isotope as a function of the energy of the incident photons.

partial photo-neutron reactions on ^{9}Be, were obtained using quasimonoenergetic annihilation photon beams and neutron multiplicity sorting method. Owing to the problem associated with experimental neutron multiplicity sorting, the partition between the extracted (γ,n) and (γ,2n) reaction cross-sections is controversial. The G4-GENBOD calculation was stopped at about 20 MeV, which is inherited from the adapted experimental data for ^{9}Be(γ,n) reaction [41]. In fact, the contribution of (γ,n) cross-section above 20 MeV is very small, and it thus can be ignored.

Comparison of G4-GENBOD calculations with EXFOR (γ,n) and (γ,2n) reaction cross-section data for ^{100}Mo and ^{100}Au in the energy range from few MeV to 30 MeV are shown in Figs. 2 and 3, respectively. The G4-GENBOD calculations are in good agreements with the experimental ones in the whole GDR region. G4PNP and G4GNR calculations are also shown in the figures, which demonstrate that the EXFOR data were reproduced with less accuracy by G4PNP and G4GNR calculations. Regarding the (γ,n) reactions for both, ^{100}Mo and ^{197}Au, the G4PNP results underestimate the EXFOR data by a factor of 0.3. The G4GNR results reproduce the magnitude of the peaked experimental cross-sections, but fail to reproduce the cross-section width. For the (γ,2n) reactions on ^{100}Mo and ^{197}Au, the EXFOR data are overestimated by both of the G4PNP and G4GNR calculations in the peak region, the discrepancy being larger for the G4GNR model. The G4PNP calculations reproduce rather well the high-energy tail of the cross-section. In summary, the data are described well within the Geant4-GENBOD approach, while the G4GNR model works better for the (γ,n) cross-section, and the G4PNP model works better for the (γ,2n) cross-section.

3.2. Neutron yield in the ^{9}Be(γ,n)^{8}Be reaction

Benchmark simulations of the neutron yield for ^{9}Be(γ,n)^{8}Be reactions were performed for validation of the Geant4-GENBOD approach. Experimentally, an 8.96 MeV electron beam impinging on a 1.88-mm tantalum target was used to produce bremsstrahlung γ-ray beam, which in turn irradiated the beryllium target and triggered the ^{9}Be(γ,n)^{8}Be reaction [40,42]. In Fig. 4, the photo-neutron yield is shown as a function of the beryllium target thickness. The data recorded by the CR-39 films are in accordance with those by Geiger–Müller detectors within ~10% [40]. Therefore, they are used for comparison with the calculations. Results from G4-GENBOD and G4PNP calculations are shown in Fig. 4.

The G4-GENBOD calculations describe well the experimental data, while large discrepancies are observed between the data and the G4PNP calculations. The G4PNP approach underestimates the photo-neutron yields by three orders of magnitude because it does not reproduce the experimental cross-sections for ^{9}Be(γ,n) reaction, as displayed in Fig. 1(a). Thus, the benchmark test suggests that the Geant4-GENBOD model reproduces well the photo-neutron yield in the GDR region.

3.3. Energy spectrum for the ^{6}Li(n,α)t and ^{7}Li(γ,α)t reactions

The Geant4-GENBOD approach was further employed to simulate

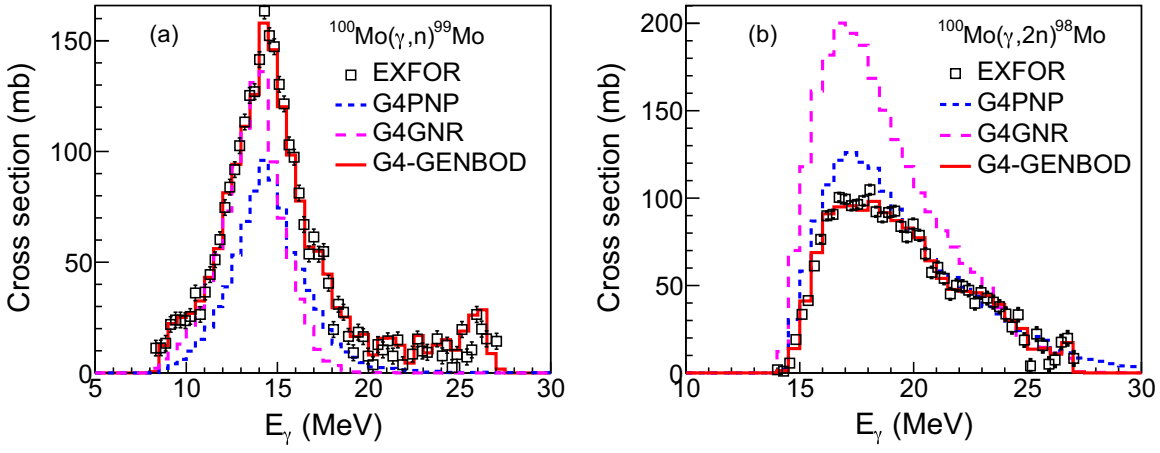

Fig. 2. Reaction cross-section for (a) the ^{100}Mo(γ, n) reaction and for (b) the ^{100}Mo(γ,2n) reaction as a function of the energy of the incident photons.

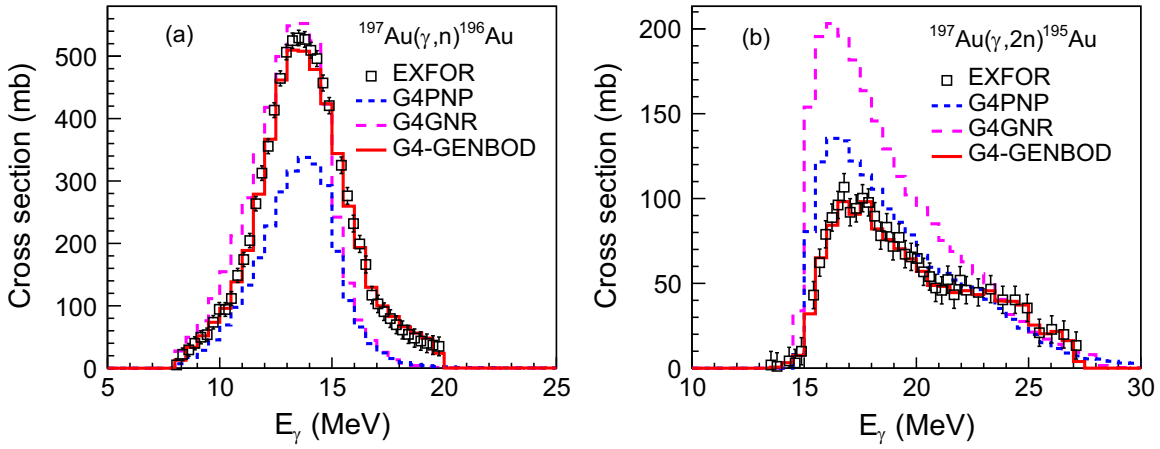

Fig. 3. Reaction cross-section for (a) the ^{197}Au(γ, n) reaction and for (b) the ^{197}Au(γ,2n) reaction as a function of the energy of the incident photons.

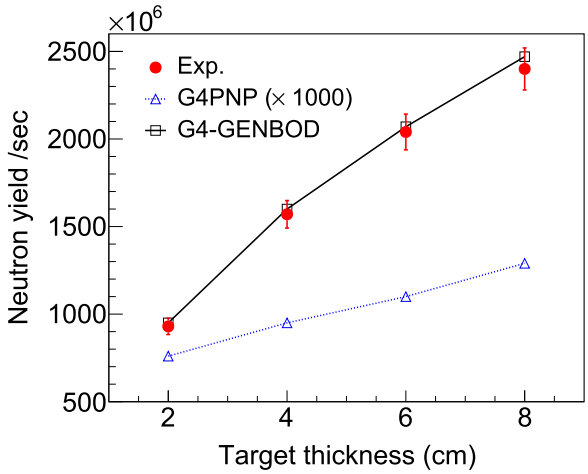

Fig. 4. Neutron yield in the ^{9}Be (γ, n) reaction *vs.* target thickness. Hollow squares and triangles denote photo-neutron yields calculated with the Geant4-GENBOD and Geant4-G4Photo Nuclear Process approaches, respectively. Filled circles are the experimental data taken from Ref [40].

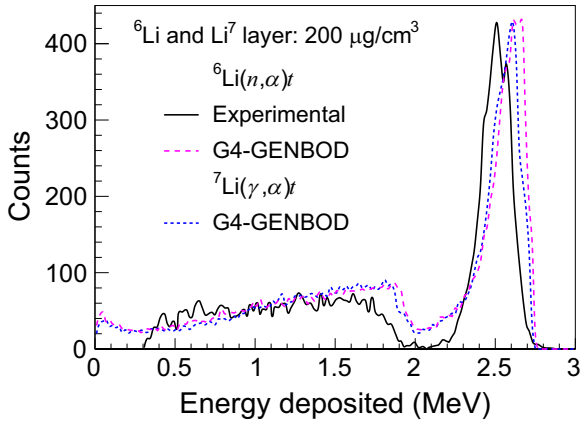

Fig. 5. Energy spectra of charged particles (tritons and α particles), measured with silicon detectors (see text for description of the detection scenario). The black solid line and the green dashed line represent the experimental measurement of Ref [43]. and the G4-GENBOD simulation for ^{6}Li(n, α)*t* reaction, respectively. The blue dashed line is the G4-GENBOD simulation for ^{7}Li(γ, α)*t* reaction. Two loci corresponding to tritons (narrow peak at 2.5 MeV) and α-particles (broad spectrum at lower energies) are clearly separated. (For interpretation of the references to color in this figure legend, the reader is referred to the web version of this article.)

the energy spectra of the ^{6}Li(n,α)*t* reaction products. Experimental data for this reaction, obtained at the neutron time-of-flight facility at CERN: n_TOF, are taken from Ref [43]. A target, consisting of a 200 μg/cm^2, enriched ^{6}Li foil sandwiched between two layers of carbon with areal density of 10 μg/cm^2, was irradiated by a neutron beam. The beam diameter was ≥2 cm diameter [43]. Silicon detectors of rectangular shape, with 6×7.5 cm^2 area and 300 μm thickness, were placed tangent to a sphere with a radius of 9.0 cm at a polar angle of 90 degrees with respect to the incident direction of the beam. The target was placed at the center of the detector assembly. This detection scenario was used in the simulations.

As a result of the neutron capture, ^{6}Li disintegrates to a triton and an alpha particle, which are detected in the experiment:

$$^{6}Li + n \rightarrow {}^{3}H\ (2.73\ \text{MeV}) + \alpha\ (2.05\ \text{MeV}), \quad (1)$$

This is the only possible decay channel following the neutron capture and it is free of γ-rays. The energy spectrum, measured with the silicon detectors, is shown in Fig. 5. The spectrum has a typical shape, and allows easy discrimination of the neuron-capture reaction products from each other. The tritons loose a small fraction of their energy inside the ^{6}Li and ^{12}C layers. As a result a peak centered at ~2.6 MeV, consistent with the value of 2.73 MeV in Eq. (1), is observed in the experimental spectrum. The spectrum of the α-particles is much broader, due to the larger energy losses in the target materials. It has a low-energy tail, which reflects the uniform in-depth production inside the ^{6}Li target. The G4-GENBOD calculations are in a reasonable agreement with the experimental observations [43]. There is a low-energy cut in the experimental spectrum due to a 100-keV hardware threshold. It should be noted that the simulated peak shifts slightly relative to the experiment, which is possibly due to the fact that the detector response was not taken into account in the calculations.

An energy spectrum for the ^{7}Li(γ,α)*t* reaction products, simulated with the Geant4-GENBOD program, is also shown in Fig. 5. In the simulation, the sandwich-like target, consisting of 200 μg/cm^2 enriched ^{7}Li foil, which was covered by two 10 μg/cm^2 carbon layers was irradiated by a γ-beam with an energy of 7 MeV, which is much larger than the 2.5-MeV photodisintegration reaction threshold. In the photodisintegration of ^{7}Li, tritons and α-particles are produced:

$$^{7}Li + \gamma \rightarrow {}^{3}H\ (2.59\ \text{MeV}) + \alpha\ (1.94\ \text{MeV}). \quad (2)$$

The calculated energy spectrum of the reaction products of the ^{7}Li(γ,α)*t* photodisintegration reaction is similar to that of the ^{6}Li(n,α)*t* reaction (see Fig. 5). This is due to fact the two reactions lead to the same reaction products with almost identical energy. This benchmark calculation demonstrates that the developed Geant4-GENBOD algorithm is suitable for the simulations of neutron-induced nuclear reactions, too.

4. Two case studies of photonuclear reactions at ELI-NP

Here we report the results of simulations for two case studies related to the emerging experimental program of the upcoming ELI-NP facility [44,45], a (γ,p) reaction of interest for the astrophysical *p*-process and (γ,n) reactions of interest for production of medical radioisotopes. The gamma-beam system [46] at ELI-NP will deliver high-brilliance narrow-bandwidth γ-beams with spectral density of 10^4 photons/s/eV, energies up to 19 MeV, and a bandwidth of ≥0.5%.

4.1. The ^{92}Mo(γ,p) reaction

The astrophysical *p*-process is an important nucleosynthesis mechanism for production of proton-rich, stable nuclides beyond iron that cannot be reached by *s*- and *r*-processes. It is suggested that the *p*-process is responsible for the observed abundance of molybdenum and ruthenium in solar system [47]. Photonuclear reactions are of key interest for the understanding the nucleosynthesis *p*-process, and the (γ,n), (γ,p) and (γ,α) reaction rates need be determined precisely. Such experiments are considered at the ELI-NP facility [48,49], which is under construction at Bucharest-Magurele, Romania, and will become operational as a user facility in 2019.

The ^{92}Mo(γ,p) and ^{92}Mo(γ,α) reactions are used as a test case for defining the sensitivity limits of ELI-NP charged-particle detection experiments. A double-layer target was used in the simulations, consisting of a 10-μm thick enriched ^{92}Mo foil facing the γ-beam and a 0.266-μm thin carbon backing. A 4π array of large-area silicon strip detectors (SSD) is under construction and will be used at ELI-NP for charged-particle detection experiments [48]. In the simulations, the target and the SSD array were assumed to be in a vacuum chamber, and 300-μm thick Si detectors were considered. The energy of the incident γ-beam was set to 15 MeV and the energy bandwidth to 1.0%, which is a conservative value for the ELI-NP γ-ray beam.

The simulated energy spectrum for protons and α-particles, produced in the ^{92}Mo(γ,p) and ^{92}Mo(γ,α) reactions, is shown in Fig. 6(a). In the spectrum, visible separation of protons from the outgoing α-particles is observed when using a thin target (*e.g.* 5 μm thick). For relatively thick target, it is helpful for the production of protons, but it has negative impacts on the disentanglements between protons and α-particles. This is caused by the considerably broadened energy spectrum of the α-particles. Pulse shape analysis (PSA) could be considered to identify the impinging light charged particles. The PSA has proved effective down to about 2 MeV, and has been achieved with neutron transmutation doped silicon detectors [50], guaranteeing high electric field uniformity within their volume. The use of position sensitive detectors might allow one to use PSA even for less uniform detectors, thus making it possible to realize particle identification. In addition, the ^{92}Mo(γ,α) reaction cross-section is almost three orders of magnitude lower than that of ^{92}Mo(γ,p), and the contamination of α-particles to the ^{92}Mo(γ,p) reaction rate can be neglected, or can be evaluated quantitatively by necessary simulations. Electron and photon induced backgrounds, resulting from Compton effect and pair production are also considered in the simulation. The background event rate is rather small [48]. The energy deposit of the background is as low as a few hundreds keV and is not shown in Fig. 6(a). The backgrounds on silicon detectors would be negligible, introducing a negligible threshold on detectors.

The proton yield can be obtained by integration of the energy spectrum of the protons, and can be studied *vs.* the target thickness, as shown in Fig. 6(b). The proton yield increased with the increase in target thickness, and reaches saturation due to the energy losses and stopping in the target. The simulation demonstrates that at a detection limit of 10 protons per day, cross-sections down to few nanobarns at beam energy E_γ ~8.5 MeV can be measured for the ^{92}Mo(γ,p) reaction.

4.2. Estimates for production of medical radioisotopes

The conditions for production of medical radioisotopes with high-brilliance γ-beams at ELI-NP [10,11,51,52] and elsewhere [8,9,53] were studied recently. The interest in the topic is related to the increasing demand for production of new medical radioisotopes and the supply shortage of radioisotopes for medical uses, *e.g.* ^{99}Mo/^{99m}Tc [54]. Here, the Geant4-GENBOD program has been used to investigate the optimal target dimensions and γ-beam parameters on achievable specific activity of radioisotopes of medical interest.

Saturation specific activity of ^{99}Mo/^{99m}Tc and ^{225}Ra/^{225}Ac radioisotopes as a function of the target geometry is shown in Fig. 7. The saturation means the value that could be achieved after a long enough irradiation integral, *e.g.* more than 5–6 times half-life of the produced isotope. The γ-beam energy used for simulation is ≤14.7 MeV and ≤12.6 MeV, respectively. It is demonstrated that the specific activity of the radioisotopes decreases as the target thickness increases. A saturation specific activity of the order of 1–2 mCi/g was achieved for thin targets (radius 1–2 mm, thickness 1 cm), assuming a γ-beam flux of 10^{11} photons/s at the ELI-NP facility. The value of the specific activity is in accordance with previous estimates, using a simple Monte Carlo simulation [17], which also takes into account experimental cross-sections [38].

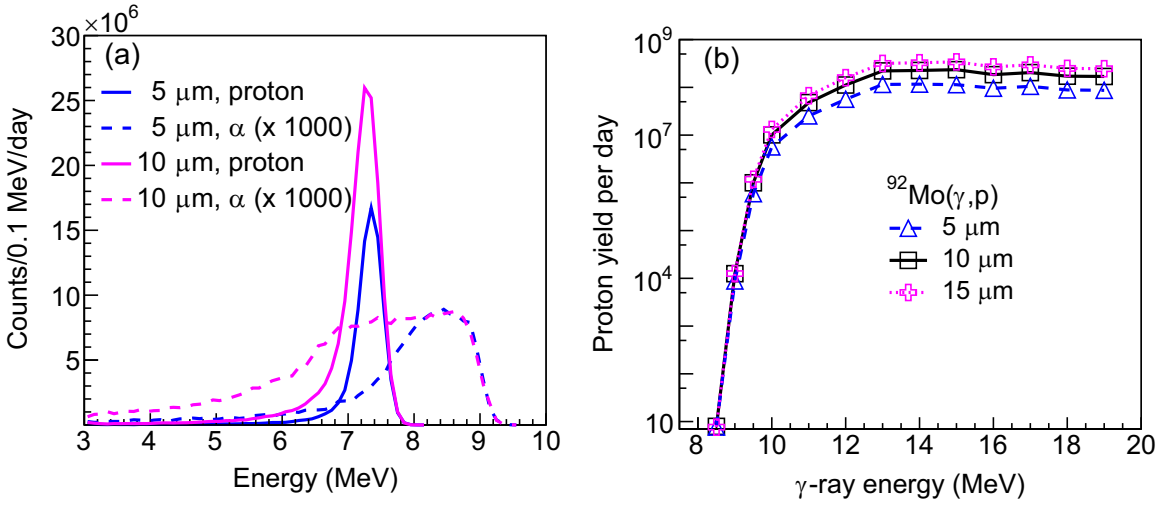

Fig. 6. (a) Particle energy spectrum resulting from ^{92}Mo(γ, p) and ^{92}Mo(γ, α) reactions induced by a 15-MeV γ-beam and (b) proton yield per day as a function of the γ-beam energy for different target thicknesses for the ^{92}Mo(γ, p) reaction. In the calculations, the γ-beam flux of 10^9 photons/s within 0.1% bandwidth is considered.

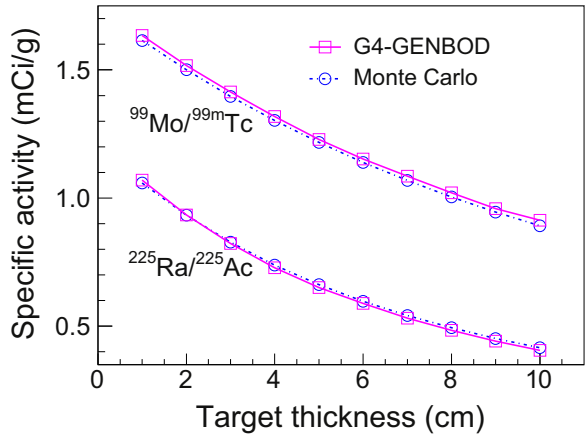

Fig. 7. Saturation specific activity of ^{99}Mo/^{99m}Tc and ^{225}Ra/^{225}Ac radioisotopes as a function of the target thickness. The radius of the irradiated target is set to 2 mm. Results of the G4-GENBOD calculation and the Monte Carlo simulation [17] are plotted with square and circular open symbols represent, respectively.

5. Summary and outlook

A data-based Monte Carlo simulation algorithm, Geant4-GENBOD, has been developed for more accurate simulations of photonuclear processes by adding the n-body Monte-Carlo event generator to our local copy of the Geant4 toolkit. The validation of the newly developed program, as the result of the algorithm, has been performed *via* comparison of calculations with reported measurements of photo-neutron production cross-sections and yields, and with reported energy spectra. Therefore, we conclude that the validation of the computer program, which is built on top of the Geant4 toolkit, is verified successfully.

The Geant4-GENBOD program is a reliable tool for simulations of photonuclear studies and various potential applications, such as photon-induced transmutation, accelerator shielding, and dosimetry calculations. Simulations for the ^{92}Mo(γ,p) reaction of astrophysics interest and (γ,n) reactions for production of medical radioisotopes were performed, which demonstrate the applicability of this approach. The Geant4-GENBOD program would be used for simulation of photonuclear experiments at high-intensity γ-beam laboratories, such as the Pan-European ELI-NP facility at Bucharest-Magurele, Romania [44,45] and the High Intensity Gamma-Ray Source at Duke University, USA [55,56].

Acknowledgements

This work is supported by the National Natural Science Foundation of China (Grant Nos. 11675075, 11405083 and 11605084), and by the Extreme Light Infrastructure Nuclear Physics (ELI-NP) Phase II, a project cofinanced by the Romanian Government and the European Union through the European Regional Development Fund - the Competitiveness Operational Programme (1/07.07.2016, COP, ID 1334). W.L. appreciates the support from the Young Talent Project of the University of South China.

References

[1] S.E. Woosley, W.M. Howard, Astrophys. J. Suppl. Ser. 36 (1978) 285–304.
[2] S. Fujimoto, M. Hashimoto, O. Koike, et al., Astrophys. J. 585 (2003) 418–428.
[3] T. Hayakawa, N. Iwamoto, T. Shizuma, et al., Phys. Rev. Lett. 93 (2004) 161102.
[4] K.W.D. Ledingham, J. Magill, P. McKenna, et al., J. Phys. D: Appl. Phys. 36 (2003) L79–L82.
[5] R. Takashima, S. Hasegawa, K. Nemoto, et al., Appl. Phys. Lett. 86 (2005) 011501.
[6] E. Irani, H. Omidvar, R. Sadighi-Bonabi, Energy Convers. Manag. 77 (2014) 558.
[7] Z.C. Zhu, W. Luo, Z.C. Li, et al., Ann. Nucl. Energy 89 (2016) 109–114.
[8] V.N. Starovoitova, L. Tchelidze, D.P. Wells, Appl. Radiat. Isot. 85 (2014) 39–44.
[9] R. Avagyan, A. Avetisyan, I. Kerobyan, et al., Nucl. Med. Biol. 41 (2014) 705–709.
[10] W. Luo, M. Bobeica, I. Gheorghe, et al., Appl. Phys. B: Lasers Opt. 122 (2016) 1–11.
[11] W. Luo, Nucl. Sci. Technol. 27 (2016) 96.
[12] F. Rahmani, M. Shahriari, Nucl. Instrum. Methods A 618 (2010) 48–53.
[13] F. Torabi, S.F. Masoudi, F. Rahmani, Ann. Nucl. Energy 54 (2013) 192–196.
[14] W.L. Huang, Q.F. Li, Y.Z. Lin, Nucl. Instrum. Methods B 229 (2015) 339–347.
[15] W.L. Huang, Q.F. Li, Y.Z. Lin, et al., Nucl. Instrum. Methods B 251 (2006) 361–366.
[16] M. Tatari, A.H. Ranjbar, Ann. Nucl. Energy 63 (2014) 69–74.
[17] W. Luo, D.L. Balabanski, D. Filipescu, Nucl. Sci. Tech. 27 (2016) 113.
[18] S. Agostinelli, J. Allison, K. Amako, et al., Nucl. Instr. Methods A 506 (2003) 250–303.
[19] J. Allison, K. Amako, J. Apostolakis, et al., IEEE Trans. Nucl. Sci. 53 (2006) 270–278.
[20] A. Fasso, A. Ferrari, J. Ranft, et al., in: Proceedings of the FLUKA, A Multi-particle Transport Code, CERN-2005-10, INFN/TC05/11, SLAC-R-773, 2005.
[21] MCNP, ⟨https://mcnp.lanl.gov⟩.
[22] J.E. McFee, A.A. Faust, K.A. Pastor, Nucl. Instrum. Methods A 704 (2013) 131–139.
[23] J.W. Shin, Nucl. Instrum. Methods B 358 (2015) 194–200.
[24] J.W. Shin, T.S. Park, Nucl. Instrum. Methods B 342 (2015) 194–199.
[25] ENDF/B-VII.1, Available online at ⟨http://www.nndc.bnl.gov/csewg/⟩.
[26] Geant4, ⟨http://geant4.cern.ch/⟩.
[27] ⟨http://geant4.cern.ch/support/proc_mod_catalog/processes/hadronic/G4PhotoNuclearProcess.html⟩.
[28] ⟨http://geant4.cern.ch/support/proc_mod_catalog/models/hadronic/G4GammaNuclearReaction.html⟩.
[29] ⟨https://geant4.web.cern.ch/geant4/support/proc_mod_catalog/cross_sections/G4PhotoNuclearCrossSection.html⟩.
[30] D.H. Wright, M.H. Kelsey, Nucl. Instrum. Methods A 804 (2015) 175–188.
[31] M.V. Kossov, Eur. Phys. J. A 14 (2002) 265–269.
[32] ⟨http://cmd.inp.nsk.su/old/cmd2/manuals/cernlib/shortwrups/node266.html⟩.
[33] F. James, Monte Carlo Phase Space, CERN, 1968, pp. 68–15.
[34] ⟨https://root.cern.ch/doc/master/classTGenPhaseSpace.html⟩.
[35] ROOT website, ⟨https://root.cern.ch/⟩.
[36] M. Herman, R. Capote, B.V. Carlson, et al., Nucl. Data Sheets 108 (2007) 2655.
[37] A.J. Koning, M. Duijvestijn, in: Proceedings of the International Conference on Nuclear Data for Science and Technology - ND2007, 2008, p. 211. See also: www.talys.eu.
[38] IAEA Nuclear Data Services, ⟨https://www-nds.iaea.org/exfor/exfor.htm⟩.
[39] H. Utsunomiya, et al., Phys. Rev. C 92 (2015) 064323.
[40] K.M. Eshwarappa, G. Sanjeev, K. Siddappa, et al., Ann. Nucl. Energy 34 (2007) 896–901.
[41] A.M. Goryachev, G.N. Zalesnyy, I.V. Pozdnev, Izv. Ross. Akad. Nauk, Ser. Fiz. 56 (1992) 159.
[42] K.M. Eshwarappa, S.K. Ganesh, et al., Nucl. Instrum. Methods A 540 (2005) 412–418.
[43] S. Marrone, et al., Nucl. Instrum. Methods A 517 (2004) 389–398.
[44] ⟨http://www.eli-np.ro/⟩.
[45] N.V. Zamfir, Nucl. Phys. News 25 (3) (2015) 34–38.
[46] O. Adriani, et al., arXiv:1407.3669v1[physics.acc-ph].
[47] M. Arnould, S. Goriely, Phys. Rep. 384 (2003) 1–84.
[48] O. Tesileanu, et al., Rom. Rep. Phys. 68 (2016) S699–S734.
[49] F. Camera, et al., Rom. Rep. Phys. 68 (2016) S539–S620.
[50] J.A. Duenas, et al., Nucl. Instr. Methods A 676 (2012) 70.
[51] M. Bobeica, D. Niculae, D. Balabanski, et al., Rom. Rep. Phys. 68 (2016) S847–S883.
[52] W. Luo, M. Bobeica, D. Filipescu, et al., Acta Phys. Pol. B 47 (2016) 763–769.
[53] B. Szpunar, C. Rangacharyulu, S. Date, et al., Nucl. Instr. Methods A 729 (2013) 41–50.
[54] P. Gould, Nature 460 (2009) 312–313.
[55] ⟨http://www.tunl.duke.edu/higs/⟩.
[56] H.R. Weller, M.W. Ahmed, Y.K. Wu, Nucl. Phys. News 25 (3) (2015) 19–24.